

## Computational Physics



# Generating and grading 34 optimised norm-conserving Vanderbilt pseudopotentials for actinides and super-heavy elements in the PseudoDojo <sup>☆</sup>

Christian Tantardini <sup>a,b,c,\*,1</sup>, Miroslav Iliaš <sup>d,e,f,1</sup>, Matteo Giantomassi <sup>g,\*,1</sup>, Alexander G. Kvashnin <sup>h</sup>, Valeria Pershina <sup>e</sup>, Xavier Gonze <sup>g,\*</sup>

<sup>a</sup> Hylleraas center, Department of Chemistry, UiT The Arctic University of Norway, PO Box 6050 Langnes, Tromsø, N-9037, Norway

<sup>b</sup> Department of Materials Science and Nonengineering, Rice University, 6100 Main St, Houston, 77005, TX, USA

<sup>c</sup> Institute of Solid State Chemistry and Mechanochemistry SB RAS, Kutateladze Street 18, Novosibirsk, 630128, Russian Federation

<sup>d</sup> Helmholtz-Institut Mainz, Staudingerweg 18, Mainz, 55099, Germany

<sup>e</sup> GSI Helmholtzzentrum für Schwerionenforschung GmbH, Planckstr. 1, Darmstadt, D-64291, Germany

<sup>f</sup> Department of Chemistry, Faculty of Natural Sciences, Matej Bel University, Tajovského 40, Banská Bystrica, 97401, Slovakia

<sup>g</sup> European Theoretical Spectroscopy Facility, Institute of Condensed Matter and Nanosciences, Université catholique de Louvain, Chemin des étoiles 8, Louvain-la-Neuve, B-1348, Belgium

<sup>h</sup> Skolkovo Institute of Science and Technology, Skolkovo Innovation Center, Bolshoy boulevard 30, Moscow, 121205, Russian Federation

## ARTICLE INFO

**Keywords:**

Optimised norm-conserving Vanderbilt pseudopotentials  
Actinides  
Super-heavy elements

## ABSTRACT

In the last decades, material discovery has been a very active research field driven by the need to find new materials for many different applications. This has also included materials with heavy elements, beyond the stable isotopes of lead, as most actinides exhibit unique properties that make them useful in various applications. Furthermore, new heavy elements beyond actinides, collectively referred to as super-heavy elements (SHEs), have been synthesized, filling previously empty space of Mendeleev periodic table. Their chemical bonding behaviour, of academic interest at present, would also benefit of state-of-the-art modelling approaches.

In particular, in order to perform first-principles calculations with planewave basis sets, one needs corresponding pseudopotentials. In this work, we present a series of scalar- and fully-relativistic optimised norm-conserving Vanderbilt pseudopotentials (ONCVPs) for thirty-four actinides and super-heavy elements, for three different exchange-correlation functionals (PBE, PBEsol and LDA). The scalar-relativistic version of these ONCVPs is tested by comparing equations of states for crystals, obtained with ABINIT 9.6, with those obtained by all-electron zeroth-order regular approximation (ZORA) calculations, without spin-orbit coupling, performed with the Amsterdam Modelling Suite BAND code.  $\Delta$ -Gauge and  $\Delta_1$ -Gauge indicators are used to validate these pseudopotentials. This work is a contribution to the PseudoDojo project, in which pseudopotentials for the whole periodic table are developed and systematically tested. The pseudopotential files are available on the PseudoDojo web-interface pseudo-dojo.org in psp8 and UPF2 formats, both suitable for ABINIT, the latter being also suitable for Quantum ESPRESSO.

## 1. Introduction

In the last decades the search for new materials incorporating actinide elements has been a hot topic. They are useful in various applications like power engineering, medicine, industry, research, etc. Some of them can form high-temperature superconducting hydrides under

high pressure [1–4]. Actinides like thorium, uranium, and plutonium actively form oxides with a band gap close to that of gallium arsenide (GaAs), making them very efficient solar cells absorbers [5,6]. Furthermore, uranium and plutonium oxides are considered to be promising for high-density integrated circuits with higher breakdown voltages [5–7] due to twice higher dielectric constant compared to GaAs (i.e., 14.1).

<sup>☆</sup> The review of this paper was arranged by Prof. Blum Volker.

\* Corresponding authors.

E-mail addresses: [christiantantardini@ymail.com](mailto:christiantantardini@ymail.com) (C. Tantardini), [matteo.giantomassi@uclouvain.be](mailto:matteo.giantomassi@uclouvain.be) (M. Giantomassi), [xavier.gonze@uclouvain.be](mailto:xavier.gonze@uclouvain.be) (X. Gonze).

<sup>1</sup> Ch.T., M.I. and M.G. contributed equally to this work.

They can be used as bipolar junction transistor due to formation of the hole (i.e., *p*-type) and electron (i.e., *n*-type) polaron levels in the band gap in the presence of oxygen defects in the interstitial space, or in the case of oxygen vacancies [8–19].

Some actinides are widely present on earth, but most are scarcely abundant and all of them are radioactive, with a reduction of their scope for applications. Notwithstanding this shortcoming, and considering more the academic interest, new opportunities appear thanks to the development and availability, even scarce, of SHEs, new heavier elements expanding the Mendeleev periodic table. In the last decades new techniques were developed to synthesize SHEs with atomic number *Z* larger than 103, approaching *Z* equal to 120. SHEs are found in *s*, *p*- and *d*-blocks of the Mendeleev periodic table. Unfortunately, SHEs have short lifetimes, which makes difficult the study of their chemistry [20–24], apart from theoretical studies.

Let us mention some of these theoretical studies, to illustrate the interesting chemistry (and physics) that might be found with these SHEs. Indeed, the chemical behaviour of two SHEs has been found to differ from what was previously expected from them: copernicium, Cn (*Z* = 112) [25–30] and oganesson, Og (*Z* = 118) [31,28,32–35].

Copernicium has electronic configuration [Rn]7s<sup>2</sup>5f<sup>14</sup>6d<sup>10</sup>. This means that it belongs to the group 12 in modern IUPAC notation. Other elements of group 12 are Zn, Cd, and Hg. If the first two are seen to be solid, the last is liquid at normal conditions. In Hg there are filled 4f orbitals close to the nucleus which lead to reduced shielding of the nuclear charge on the valence shell. This effect is called lanthanide contraction and is responsible for the high interaction between the 6s orbitals and the nucleus. The lanthanide contraction in Hg is responsible for its liquid state at normal conditions. In Cn (*Z* = 112) the contraction affects the orbital energies, making energies of 5f-orbitals closer to 6d-orbitals. This distinguishes Cn from the other elements of group 12 [25–30,36].

The other is oganesson Og (*Z* = 118), the only super-heavy element that belongs to the noble gases family (i.e. group 18 of the periodic table according to IUPAC notation). Og is expected to be a colourless, odourless, tasteless, non-flammable gas like all other noble gases. However, the most important aspect of all noble gases is that they have a fully occupied outer electronic shell, which makes them reluctant to participate in chemical reactions under normal conditions. In the last decades the field of high-pressure chemistry has shaken the established chemistry of noble gases, revealing new compounds with helium, sodium and others [37–45], like the Na<sub>2</sub>He stable crystal at pressure higher than 135 GPa [37–39]. Furthermore, new highly reactive compounds could be obtained from noble gases by photo-chemical reaction: fluorides like XeF<sub>2</sub> and KrF<sub>2</sub>, or oxides like XeO<sub>3</sub> [46]. In fact, Og (*Z* = 118) appears to form charged hydrides, fluorides and diatomic molecules with itself under various environmental conditions, making this element attractive for its high reactivity relative to the other noble gases. [31,28,32–34,36].

The chemical bonding of (most) actinides and SHEs with other elements has only been studied at the molecular level, albeit by all-electron (AE) approaches with complex relativistic post-Hartree-Fock methodologies and large local basis sets. If post-Hartree-Fock approaches are fruitfully employed in gas phase they cannot be accurately employed for periodic systems. In fact, quantum chemical calculations for condensed matter usually rely on planewaves basis sets [47], where the core electrons of each atom are frozen and the divergence of Coulombic nuclear potential at the center of nucleus is avoided thanks to the use of a smooth pseudopotential. Therefore, large periodic systems of actinides or SHEs are rarely studied with a planewave basis set due to the scarcity of pseudopotentials tailored for elements with *Z* greater than 100.

Furthermore, actinides present a spatial extension of 5f-orbitals comparable to 6d-orbitals. This means that the chemical bonding of actinides cannot be described if 5f-electrons are frozen in the core, but they must be described by pseudowavefunctions in the valence shell, making more difficult the generation of pseudopotentials. This is at variance with the one of 4f electrons of the lanthanides, that for some

materials can be frozen within the core of pseudopotential due to their smaller extension with little spatial overlap with the 5d-electrons. Thus, the developed pseudopotentials for actinides and SHEs should be characterised by numerous semicore states in the valence shell in order to increase the transferability of pseudopotential. Such a warning applies to all pseudopotential formalisms, including the Projector-Augmented Wave (PAW) method, all giving uncontrolled error in the presence of overlap between pseudospheres. [48] As an example, in presence of overlap between the PAW pseudospheres, the computed electric field gradients might have an error on the order of 10<sup>-1</sup> MHz, with unreliable sign [49]. ONCVPs with semi-core states and small pseudocore radii can avoid such problems. Moreover, ONCVPs open the possibility to use complex approaches as *GW* approximation [50], Bethe–Salpeter equation [51] and electron-phonon coupling [52] for advanced studies of solid-state crystals.

Thus, in the present work we continue the PseudoDojo project (web interface at [pseudo-dojo.org](http://pseudo-dojo.org)) started in 2018 [53], in which ONCVPs were proposed for 85 elements. The PseudoDojo project includes a Python framework for automatic generation and validation of pseudopotential properties. It consists of three different parts: (1) a database of reference results obtained with AE (i.e. Gaussian orbital basis set) and planewave basis set codes; (2) a set of tools and graphical interfaces to facilitate the generation and initial validation of the pseudopotentials; (3) a set of scripts to automate the execution of the various periodic structure tests with the ABINIT code.

Here, we provide a set of fully-relativistic closed-shell ONCVPs for actinides and SHEs. The precision of the developed ONCVPs is tested at the scalar-relativistic level by comparison with AE references, for monoatomic face-centered cubic primitive cells, based on the  $\Delta$ -Gauge [54] and  $\Delta_1$ -Gauge [55] descriptors. The relative error for  $V_0$  and  $B_0$  between planewave and AE calculations is also shown.

## 2. Methods

### 2.1. Generating the pseudopotentials

ONCVPs have been generated using the version 4.0.1 of the ONCVPSP package, available at [github.com/oncvpsp/oncvpsp](https://github.com/oncvpsp/oncvpsp). As mentioned in the previous section, design choices were such that a relatively large set of orbitals were chosen as semi-core states, in order to obtain good transferability and applicability of the generated pseudopotentials. Associated with this design choice, the chosen cut-off radii have to be quite small.

Although the details of the ONCVP generation are given in Ref. [56, 57], some characteristics are worth to mention here. To improve the transferability of pseudopotentials, we rely on Non-Linear Core Corrections (NLCC) [58]. NLCC removes the non-physical oscillations of the local potential  $\hat{V}_{loc}$  (i.e., the potential coming from the projectors used to generate the pseudopotential), which must coincide with the AE potential  $V_{AE}$  outside the pseudopotential cut-off radii  $r_c$  [56,57]. Specifically, actinides are expected to have strong oscillation of the potential close to the nucleus, coming from the presence of 5f-electrons in the valence shell. We have used Teter NLCC [59] that allowed us to obtain smooth core charges with a consequent reduction in the kinetic energy cut-off required to obtain e.g. phonon convergence for the acoustic phonon branches.

Each channel corresponding to one specific *l*-state is characterised by its number of projectors, its cut-off radii, its number of Bessel functions and its cut-off wavevector of Bessel functions [56,57]. We provide such data in the Supporting Information, namely one table for each element, numbered ST.1 to ST.34. The overall cut-off radius of the pseudopotential is the largest of the channel cut-off radii.

The number of projectors depends on the chosen valence electronic configuration and usually corresponds to the number of states for a specific angular momentum channel. In some SHEs an unbounded *f*-projector was added to improve the quality of pseudopotential. The

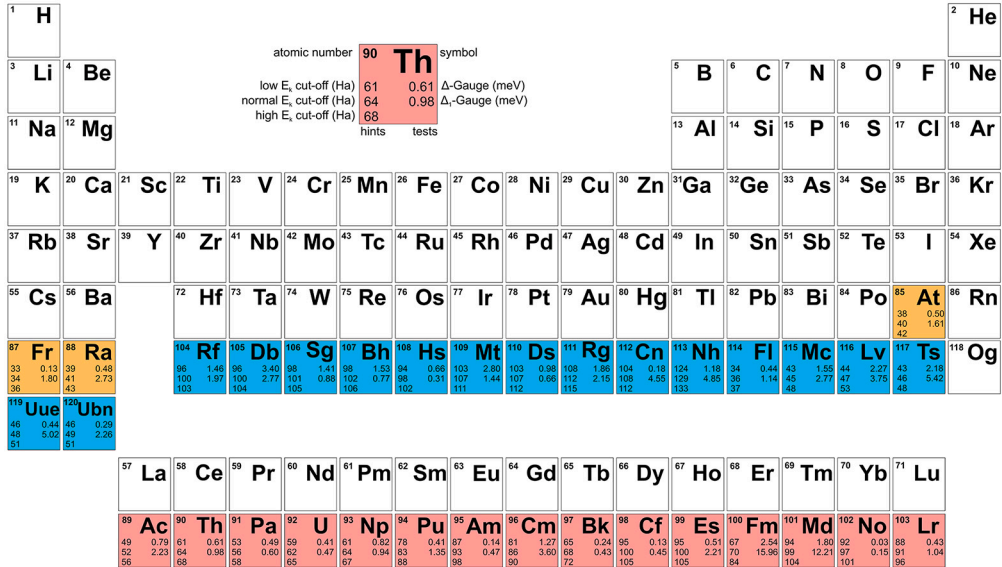


**Fig. 1.** Periodic table showing the 34 elements for which ONCVPs are developed in the present work. Actinides are highlighted in red, SHEs in blue, and Fr, Ra and At in orange. For each element, the atomic number and symbol are mentioned in the upper part of the cell. In the lower left part of the cell, hints for kinetic energy cut-off are given, in Hartree. In the lower right part of the cell, the Δ-Gauge and normalised Δ<sub>1</sub>-Gauge values are given, both in meV.

number of projectors as all other parameters chosen for the generation of a specific pseudopotential are given at the end of pseudopotential file for both formats psp8 and UPF2.

The number of projectors being defined, we have initially individually searched for each channel the cut-off radius that allows the pseudowavefunction to match the last maximum (or minimum) of the AE wavefunction, and we chose the necessary number of Bessel functions and their cut-off radii to allow the convergence of projectors so to obtain a good match for the logarithm derivative for  $\ell$ -state with respect to the energy between the pseudowavefunction and the AE wavefunction. At the end, all channels are considered together for the final refinement of the pseudopotential. They are interconnected, because the variation of parameter of a channel inevitably affects the others. The channel parameters are thus tuned in order to obtain both good Δ-Gauge and low planewave kinetic energy cut-off for the total energy. The parameters for the Teter model charge, [56,57] which are called amplitude prefactor and scale prefactor, are initially chosen automatically by Nelder-Mead simplex algorithm [59] and subsequently manually adjusted to have a smoother model charge with consequent reduction of the needed kinetic energy cut-off and more stability of phonon calculations.

Optimisation in this many-dimensional space (on the order of ten adjustable parameters, the prior choice of number of projectors per channel being understood) is non-trivial. However, the task is critically split between separate channels first, for which only few parameters need to be tuned concurrently. Instead of trying to rely on non-linear optimisation as attempted by Hansel and coworkers [60], we relied on human-driven optimisation, made efficient thanks to rich and fast graphical representation tools, available in the PseudoDojo project [github.com/PseudoDojo](https://github.com/PseudoDojo). The pseudopotential files are available in the PseudoDojo project (web interface at [pseudo-dojo.org](https://pseudo-dojo.org)), see the “Data availability statement” section.

## 2.2. Spin-orbit coupling

Two ONCVP versions are proposed for each element shown in the Mendeleev periodic table seen in the Fig. 1: scalar-relativistic and fully-relativistic pseudopotentials. Because in pseudopotential calculations with plane waves, the deepest electronic states are not treated, the four-component fully-relativistic electronic wavefunction that describes electron (i.e. positive eigenvalues) and minority contributions from

positrons (i.e. negative eigenvalues) in the fully-relativistic Dirac approach can be reduced to two components, where only the electronic (majority) contributions are explicitly described [61,62]. For such pseudopotential calculations, the scalar-relativistic case differs from the fully-relativistic one only by the presence of spin-orbit coupling in the latter. Both versions of the developed ONCVPs are referred to as “stringent” on the basis of their accuracy, following the same notation used in the previous PseudoDojo paper [53].

## 2.3. Grading the pseudopotentials

The Δ-Gauge is a well-established method to cross-compare two first-principles numerical implementations. It was formulated by Lejaeghere et al. [54], who pointed that there is no absolute reference against which to compare results from planewaves implementations with different type of pseudopotentials or from different all-electron implementations, all differing in practice by various numerical approximations, none being approximation-free. The Δ-Gauge quantifies the difference between two DFT-predicted equations of state  $E(V)$  for some system (represented by the  $i$  subscript) in the following way:

$$\Delta_i(a, b) = \sqrt{\frac{\int_{0.94V_{0,i}}^{1.06V_{0,i}} (E_{b,i}(V) - E_{a,i}(V))^2 dV}{0.12V_{0,a,i}}}, \quad (1)$$

where  $\Delta_i(a, b)$  is the root-mean-square difference between the  $E(V)$  of methods  $a$  (i.e., the reference approach) and  $b$ , over a ±6% interval around the equilibrium volume  $V_{0,a,i}$  obtained with the reference approach (i.e. the  $a$  method). Thus, having chosen one approach as the reference, the total energy is computed for the same volumic range  $E(V)$  for both approaches and compared.

However, in practice, the integral in this equation is evaluated through numerical means, using energies from seven equally spaced volumes, from 94% to 106% of the reference  $V_0$  by steps of 2%, to provide a fit using the Birch-Murnaghan [63] equation of state for each approach. This was not made explicit in the original publication [54]. The actual protocol followed in the PseudoDojo project relies on scripts available in the “Delta calculation package”, version 3.1, available at the end of the [molmod.ugent.be/deltacodesdft](http://molmod.ugent.be/deltacodesdft) Web page. The script eosfit.py allows one to compute the Birch-Murnaghan [63] equation of states and its parameters as equilibrium volume  $V_0$ , bulk modulus  $B_0$  and the first derivative of the bulk modulus with respect to pressure  $B'_0$ .

These parameters are used by `calcDelta.py` to solve numerically the integral within Eq. (1) and finally compute the  $\Delta$ -Gauge.

Another validation parameter, called normalised  $\Delta$ -Gauge, denoted by the symbol  $\Delta_1$ -Gauge, [55] is also presented,

$$\Delta_1\text{-Gauge} = \frac{V_{ref} B_{ref}}{V_{AE} B_{AE}} \Delta\text{-Gauge}. \quad (2)$$

$\Delta_1$ -Gauge is a scaled value of  $\Delta$ -Gauge with respect to a reference material having a specific equilibrium volume  $V_{ref}$  and bulk modulus  $B_{ref}$  to allow comparison between all elements. These reference values (i.e.  $V_{ref}$  and  $B_{ref}$ ), chosen from the of  $V_0$  and  $B_0$  for 71 elements, are 30 Bohr<sup>3</sup> and 100 GPa respectively. They were fixed in the previous work by Jollet et al. [55]. Keeping this definition, that does not include actinides and SHEs nevertheless, makes sense since this is in any case just choosing a reference value for the volume and the bulk modulus.

The scalar-relativistic approximation [61,62] used in pseudopotential planewave calculations is comparable with the zero-order regular approximation [64–68] (ZORA) to the full relativistic Hamiltonian, however considered without spin-orbit coupling. We have produced scalar-relativistic ONCVPs and validated their results with those of the ZORA AE calculations without spin-orbit coupling. Hereafter, when we write ZORA, we refer to AE calculations done with the scalar-relativistic approximation without spin-orbit coupling. Neither in the pseudopotentials case nor in the AE case a so-called non-relativistic treatment is done.

Nevertheless, fully-relativistic versions of the pseudopotentials are delivered, in addition to these validated scalar-relativistic pseudopotentials. Indeed, spin-orbit coupling plays an important role for actinides and SHEs and it is the suggested version for any planewave calculation that involves these elements. The scalar-relativistic version is only presented for their validation.

The validation between AE and pseudopotential results for calculations including spin-orbit coupling has been considered as well. However, several considerations prevented us for doing so. First, this comparison would have introduced an additional source of difficulty for the comparison between pseudopotentials calculations and AE ones. Second, this was not the methodology followed for the PseudoDojo and  $\Delta$ -Gauge projects, that relied on scalar-relativistic calculations for both the AE and the pseudopotential (or PAW) cases. Finally, the specific effect of spin-orbit coupling might not be best tested by examining the total energy or an equation of state. At variance, Huhn and Blum [69] have computed spin-orbit splittings at selected points in the Brillouin Zone, and compared two AE codes, FHI-aims and WIEN2K. One might as well consider to study the magnetic anisotropy, specifically for magnetic materials. We feel this interesting question might be worth a separate study.

### 3. Computational details

To validate the newly generated pseudopotentials, crystals with a face-centered cubic primitive cell containing one atom per cell are considered. DFT calculations are performed with the PBE functional, [70] the most used XC functional for the validation of pseudopotentials for periodic structures. Note however, that ONCVPs have been generated also with the PBEsol and LDA exchange-correlation functionals.

#### 3.1. All-electron calculations (AE)

ZORA AE calculations [64–68] are performed with the BAND software application from the Amsterdam Modelling Suite [71–76]. The primitive cell is optimized using the Broyden-Fletcher-Goldfarb-Shanno (BFGS) optimization algorithm [77–80]. Fermi-Dirac smearing with temperature equal to 0.001 Ha is used in all calculations. The Brillouin zone is sampled with a 15×15×15 k-point grid centered in  $\Gamma$ -point. AE calculations are performed with local Gaussian basis set triple zeta plus

**Table 1**

Equilibrium volume  $V_0$  of the Birch-Murnaghan [63] equation of state, from AE calculations (BAND code) and PW calculations using pseudopotentials from the present work - scalar-relativistic case (ABINIT code). Data from VASP are also provided, for the available PAW atomic datasets, see Methods section. The relative errors (re) with respect to the AE reference are also shown.

Atom	Z	$V_0^{AE}$ / Å <sup>3</sup>	$V_0^{PW}$ / Å <sup>3</sup> (ABINIT)	$V_0^{re}$ / % (ABINIT)	$V_0^{PW}$ / Å <sup>3</sup> (VASP)	$V_0^{re}$ / % (VASP)
At	85	39.048	38.922	-0.323	-	-
Fr	87	117.023	116.730	-0.250	-	-
Ra	88	72.205	71.908	-0.411	-	-
Ac	89	45.686	45.569	-0.256	45.474	-0.463
Th	90	32.309	32.296	-0.040	32.065	-0.756
Pa	91	25.318	25.370	0.205	26.688	5.412
U	92	21.777	21.791	0.064	21.809	0.146
Np	93	19.363	19.363	0.000	19.356	-0.035
Pu	94	28.037	27.986	-0.182	26.703	-4.757
Am	95	34.634	34.623	-0.032	32.673	-5.662
Cm	96	30.818	31.001	0.594	30.567	-0.814
Bk	97	18.282	18.248	-0.186	-	-
Cf	98	24.905	24.904	-0.004	24.048	-3.442
Es	99	23.022	23.078	0.243	-	-
Fm	100	27.631	28.329	2.526	-	-
Md	101	33.639	34.290	1.935	-	-
No	102	39.535	39.532	-0.008	-	-
Lr	103	30.064	30.023	-0.136	-	-
Rf	104	24.635	24.724	0.361	-	-
Db	105	21.282	21.373	0.428	-	-
Sg	106	18.947	18.935	-0.063	-	-
Bh	107	17.479	17.458	-0.120	-	-
Hs	108	16.706	16.694	-0.072	-	-
Mt	109	16.879	16.838	-0.243	-	-
Ds	110	18.145	18.124	-0.116	-	-
Rg	111	21.075	21.132	0.270	-	-
Cn	112	43.124	42.738	-0.895	42.839	-0.661
Nh	113	36.746	37.065	0.868	36.536	-0.571
Fl	114	37.275	37.223	-0.140	37.444	0.453
Mc	115	37.570	37.414	-0.415	37.686	0.309
Lv	116	38.033	37.797	-0.621	38.433	1.051
Ts	117	43.312	42.876	-1.007	43.605	0.677
Uue	119	100.652	99.874	-0.773	-	-
Ubn	120	78.470	78.543	0.093	-	-

double polarisation basis set describing the virtual orbital space. The convergence criterion of self-consistent total energy is  $1.0 \cdot 10^{-6}$  Ha.

#### 3.2. Planewaves basis set calculations

Planewaves basis set calculations with PBE [70] DFT functional are performed with ABINIT [81–83], for the validation of the ONCVPs, and with VASP [84–87], for comparison with prior existing PAW data, using the same parameters for the electronic smearing and BZ sampling as those used for BAND. The kinetic energy cut-off for each element is determined individually for each developed ONCVP. For PAW, one relies on the atomic dataset from Torres et al. [88,89] for the actinides, and Trombach et al. [90] for the SHE p-elements. No other PAW for SHEs had been made available to our knowledge. We use the highest kinetic energy cut-offs suggested by VASP for actinides, and suggested by Trombach et al. [90] for SHEs. The total energy convergence criterion cut-off is equal to  $1.0 \cdot 10^{-6}$  Ha.

### 4. Results and discussion

Following the methodology described in Sec. 2, we have generated pseudopotentials for the actinides and SHEs, for both scalar-relativistic and fully-relativistic cases, and for the PBE, PBEsol and LDA exchange-correlation functionals. For their availability, see the “Data availability statement” section. The validation presented in what follows, is done for the scalar-relativistic case, and using the PBE functional.

The equilibrium volume  $V_0$  (see Table 1) and the bulk modulus  $B_0$  (see Table 2) are compared from the two EOSs through the relative

**Table 2**

Bulk modulus  $B_0$  of the Birch-Murnaghan [63] equation of state from AE calculations (BAND code) and PW calculations using pseudopotentials from the present work - scalar-relativistic case (ABINIT code). Data from VASP are also provided, for the available PAW atomic datasets, see Methods section. The relative errors (re) with respect to the AE reference are also shown.

Atom	Z	$B_0^{AE}$ / GPa	$B_0^{PW}$ / GPa (ABINIT)	$B_0^{re}$ % (ABINIT)	$B_0^{PW}$ / GPa (VASP)	$B_0^{re}$ % (VASP)
At	85	24.516	24.209	-1.252	-	-
Fr	87	1.942	1.922	-1.030	-	-
Ra	88	7.022	7.281	3.688	-	-
Ac	89	23.746	23.207	-2.270	16.817	-29.179
Th	90	55.211	57.883	4.840	58.109	5.249
Pa	91	95.267	95.144	-0.129	10.474	-89.005
U	92	116.235	116.464	0.197	115.745	-0.421
Np	93	136.602	135.551	-0.769	136.401	-0.147
Pu	94	31.262	32.851	5.083	32.067	2.574
Am	95	24.992	25.550	2.233	16.797	-32.792
Cm	96	31.597	34.101	7.925	33.759	6.842
Bk	97	88.695	92.014	3.742	-	-
Cf	98	36.450	36.191	-0.711	39.807	9.210
Es	99	31.242	30.014	-3.931	-	-
Fm	100	19.335	16.856	-12.821	-	-
Md	101	12.712	12.952	1.888	-	-
No	102	13.887	13.644	-1.750	-	-
Lr	103	39.098	41.384	5.847	-	-
Rf	104	96.648	89.867	-7.016	-	-
Db	105	170.686	171.898	0.710	-	-
Sg	106	265.525	252.763	-4.806	-	-
Bh	107	345.795	339.819	-1.728	-	-
Hs	108	384.175	377.751	-1.672	-	-
Mt	109	347.424	345.757	-0.480	-	-
Ds	110	256.470	246.644	-3.831	-	-
Rg	111	118.939	122.504	2.997	-	-
Cn	112	2.728	2.847	4.362	2.704	-0.878
Nh	113	19.103	19.727	3.267	19.371	1.403
Fl	114	32.242	31.178	-3.300	33.128	2.747
Mc	115	46.125	45.017	-2.402	44.754	-2.973
Lv	116	47.214	48.112	1.902	45.542	-3.541
Ts	117	26.811	28.105	4.826	27.450	2.384
Uue	119	2.574	2.612	1.476	-	-
Ubn	120	5.777	4.917	-14.887	-	-

errors between the values predicted by ONCVP and AE data. For each element considered, the  $\Delta$ -Gauge parameter calculated with the high kinetic energy cut-off is shown in the Mendeleev periodic table, Fig. 1. As in the PseudoDojo project, the *low*, *normal* and *high* cut-off kinetic energies (Ha) for the planewave basis set are presented in the Mendeleev periodic table (see Fig. 1) to give guidance to the user. The first one (*low*) is used for a quick calculation or as a starting point for the convergence studies. The second one (*normal*) is used as a good guess for high-throughput calculations. The third one is the cut-off beyond which no significant changes in the results should be observed.

The validity of the newly developed ONCVPs has also been checked by searching for additional highly-localised positive-energy states (see Table 3), so-called “ghost states”. [91,92] In some cases, ghost states at high energies are indeed observed. When pseudopotentials are used to calculate properties that require an accurate description of the unoccupied region, i.e. optical properties or  $GW$  calculations, ghost states must be avoided below 100 eV above the Fermi level. In many cases it was possible to remove ghost states by tuning the characteristics of the second projector. It has also been found that adding more semicore states improves the quality of the logarithmic derivative at high energies. Note that the ghost states listed in Table 3 are observed at an energy high enough for not causing any problems.

#### 4.1. Elements with s highest (partly) filled shell

The elements with s highest (partly) filled shell are Fr( $Z=87$ ), Ra( $Z=88$ ), Uue( $Z=119$ ), and Ubn( $Z=120$ ). The two latter ones, Uue( $Z=119$ ) and Ubn( $Z=120$ ), are SHEs and are the last synthe-

**Table 3**

List of elements for which the pseudopotential exhibit high positive-energy ghost states.  $\epsilon$  gives the energy (eV) at which the ghost appears in the corresponding  $s$  or  $p$  channels. No ghosts are found at lower energies. The lowest ghost appearing below 130 eV, the safe energy region is sufficiently large for the reliability of electronic ground state calculations, but also electronic excitations of moderate energy, including optical properties.

Atom	Z	$\epsilon_{s-orb}$ / eV	$\epsilon_{p-orb}$ / eV
Ac	89	208.22	-
Th	90	242.59	-
Pa	91	225.71	-
U	92	225.40	-
Np	93	225.03	-
Pu	94	264.98	-
Am	95	351.10	-
Cm	96	266.93	-
Bk	97	266.23	-
Cf	98	265.48	-
Es	99	264.68	-
Mc	115	133.96	-
Lv	116	134.80	165.53
Ts	117	135.63	-
Ubn	120	156.73	-

sized elements [93,94]. The mere specification of the  $s$  valence shell with a pseudowavefunction is not sufficient to correctly describe the chemistry of these elements at high pressures [37,95,96], as  $d$  semicore states are involved in chemical bonding [37,95,96]. Thus, valence configurations  $5s^25p^65d^{10}6s^26p^67s^1$  for Fr( $Z=87$ ) and  $5s^25p^65d^{10}6s^26p^67s^2$  for Ra( $Z=88$ ) have been used. Similarly, valence configurations  $6s^26p^66d^{10}7s^27p^68s^1$  for Uue( $Z=119$ ) and  $6s^26p^66d^{10}7s^27p^68s^2$  for Ubn( $Z=120$ ) have been used. In particular, an improvement of the  $\Delta$ -Gauge has been observed by introducing two projectors for the empty  $6f$  orbitals in Fr( $Z=87$ ) and two projectors for the empty  $7f$  orbitals in Uue( $Z=119$ ).

#### 4.2. Element with p highest (partly) filled shell

At( $Z=85$ ) was predicted by Niels Bohr as the 5<sup>th</sup> halogen in the Mendeleev periodic table [97]. Dmitri Mendeleev in his work left an empty space on At( $Z=85$ ) position. Such element has been synthesized in laboratory by bombarding bismuth-209 with alpha particles [97], for the first time in 1940. In recent decades, with the need to find new materials, At( $Z=85$ ) has been found to be a promising element for the development of radiopharmaceuticals [98–101]. No pseudopotential for At had been proposed in the 2018 set from the PseudoDojo project, and this omission is removed in the present work, in order to increase the possibility of new studies on its chemistry and possible compounds. Here the valence shell configuration is  $5s^25p^65d^{10}5f^{14}6s^26p^5$ , adding also two projectors for the empty  $5f$  orbitals in order to increase the transferability of the pseudopotential.

The other  $p$ -elements considered in this work are the SHEs Nh( $Z=113$ ) Fl( $Z=114$ ) Mc( $Z=115$ ), Lv( $Z=116$ ) and Ts( $Z=117$ ). If the  $p$ -elements of the 6<sup>th</sup> series are subjected to the lanthanide contraction due to the presence of filled  $4f$ -orbitals which allow them to freeze in the nucleus as they are close to it, the SHEs of the 7<sup>th</sup> series are characterised by filled  $5f$ -orbitals which are more spatially extended than the  $4f$ -orbitals. So  $5f$  orbitals have been introduced into the valence shell, making it look like  $5s^25p^65d^{10}5f^{14}6s^26p^66d^{10}7s^27p^{1-5}$  for all of them.

Unfortunately we have not succeeded in developing a decent ONCVP for Og(118), sufficiently accurate ones being generated only with an important increase of the kinetic energy cut-off.

**Table 4**

For actinides, valence shell (including semi-core states) of present work ONCVPs and valence shell of PAW VASP atomic data. The latter did not contain the details of the valence shell for elements from Ac to Pu. In this case we have indicated only the declared number of electrons. One might hypothesize that the 6s, 6p and 7s shells of these elements are complete, leaving the incomplete 5f shell for the remaining electrons.

Atom	Z	ONCVP Valence shell	PAW Valence shell
Ac	89	$5s^2 5p^6 5d^{10} 6s^2 6p^6 6d^1 7s^2$	(11e <sup>-</sup> )
Th	90	$5s^2 5p^6 5d^{10} 5f^2 6s^2 6p^6 6d^1 7s^2$	(12e <sup>-</sup> )
Pa	91	$5s^2 5p^6 5d^{10} 5f^2 6s^2 6p^6 6d^1 7s^2$	(13e <sup>-</sup> )
U	92	$5s^2 5p^6 5d^{10} 5f^3 6s^2 6p^6 6d^1 7s^2$	(14e <sup>-</sup> )
Np	93	$5s^2 5p^6 5d^{10} 5f^4 6s^2 6p^6 6d^1 7s^2$	(15e <sup>-</sup> )
Pu	94	$5s^2 5p^6 5d^{10} 5f^5 6s^2 6p^6 6d^1 7s^2$	(16e <sup>-</sup> )
Am	95	$5s^2 5p^6 5d^{10} 5f^6 6s^2 6p^6 6d^1 7s^2$	$5f^7 6s^2 6p^6 7s^2$
Cm	96	$5s^2 5p^6 5d^{10} 5f^7 6s^2 6p^6 6d^1 7s^2$	$5f^6 6s^2 6p^6 6d^2 7s^2$
Bk	97	$5s^2 5p^6 5d^{10} 5f^8 6s^2 6p^6 6d^1 7s^2$	-
Cf	98	$5s^2 5p^6 5d^{10} 5f^9 6s^2 6p^6 6d^1 7s^2$	$5f^8 6s^2 6p^6 6d^2 7s^2$
Es	99	$5s^2 5p^6 5d^{10} 5f^{10} 6s^2 6p^6 6d^1 7s^2$	-
Fm	100	$5s^2 5p^6 5d^{10} 5f^{12} 6s^2 6p^6 7s^2$	-
Md	101	$5s^2 5p^6 5d^{10} 5f^{13} 6s^2 6p^6 7s^2$	-
No	102	$5s^2 5p^6 5d^{10} 5f^{13.90} 6s^2 6p^6 6d^1 7s^2$	-
Lr	103	$5s^2 5p^6 5d^{10} 5f^{14} 6s^2 6p^6 6d^1 7s^2$	-

#### 4.3. Element with d highest (partly) filled shell

SHEs with d highest (partly) filled shell, similarly to the SHEs with p highest (partly) filled shell, are characterised by large filled 5f-orbitals which require their inclusion in the valence shell. The series starts at Rf(Z = 104) and ends at Cn(Z = 112). Their valence configuration is chosen to be  $5s^2 5p^6 5d^{10} 5f^{14} 6s^2 6p^6 6d^{1-10} 7s^2$ . The 6d-elements are characterised by  $6d^{1-10} 7s^2$  orbitals close in energy which are systematically involved in chemical bonding. By including such extended semicore states we are confident of adequately describing the chemistry of such elements.

Triggered by the presence of ferromagnetic ordering for lighter elemental solids with d highest (partly) filled shell, we have investigated the possibility to find a ferromagnetic ground state, for the FCC primitive cell, using AE calculations. This was also done for other SHEs and actinides. None of SHEs showed such a magnetic behaviour. This agrees with the relatively large spatial extension of partially filled 6d-orbitals. In the literature, we have not seen an investigation of the magnetic order for SHEs until now of their solid phase.

#### 4.4. Actinides

Actinides, with Z from 89 to 103, are characterised by the presence of 5f-electrons that play a major role in the chemical bonding. This differs from their lanthanide counterparts, the 5f-orbitals having a large spatial extension, unlike lanthanide 4f-orbitals. Indeed, 4f-orbitals are close to the nucleus and can often be frozen within the core, for materials in which the lanthanide has an oxidation state of III. [53]

In the actinide series additional 5f-orbitals are not systematically filled with increasing Z. In fact we had to tailor the ONCVPs for the specific known valence shell of each actinide (see Table 4)

The presence of partly filled 5f-orbitals often induces magnetism of actinide-based materials. As a consequence, the magnetism of the FCC elemental crystal has been checked for each actinide, by performing ferromagnetic AE ZORA calculations [64–68], see Table 5. In this table, it is seen that ten actinides exhibit magnetic behaviour within the FCC primitive cell. This brought us to consider whether pseudopotential and AE EOS should be compared for the non-magnetic case or, instead, for the magnetic case.

Several concerns are present. The  $\Delta$ -Gauge project relies only on EOS for the non-magnetic case, even for transition metals. This would favour relying on such non-magnetic EOS for actinides as well, for consistency reasons. However, the  $\Delta$ -Gauge project did not include

**Table 5**

Magnetic moment of actinides within FCC phase, in  $\mu B$ , calculated with ZORA AE calculations using atomic Hirshfeld partition.

Atom	Z	Hirshfeld mag. / $\mu B$
Ac	89	-
Th	90	-
Pa	91	-
U	92	-0.892
Np	93	-2.695
Pu	94	-5.785
Am	95	-7.321
Cm	96	-7.026
Bk	97	-5.459
Cf	98	-4.164
Es	99	-2.906
Fm	100	-1.643
Md	101	-0.419
No	102	-
Lr	103	-

rare-earth elements with f highest (partly) filled shell, for which the magnetism is particularly strong. One can wonder whether studying EOS of non-magnetic phases of these materials is relevant at all. The choice to restrict to non-magnetic EOS might not be completely pertinent not only for rare-earth elements, but also for the present actinides.

This being said, the specific choice of the FCC phase might anyhow bias the presence of magnetism. On a more practical point of view, it was also observed that the determination of the AE EOS for several actinides is not straightforward due to the presence of two electronic phases in the magnetic case: the system jumps from one to the other, in the volume region where the energy is minimal, making difficult the application of the usual protocol to find the  $\Delta$  factor.

Finally, we decided to stick to the non-magnetic treatment with most materials, with the exception of Pu(Z = 94), Am(Z = 95), Cm(Z = 96) and Cf(Z = 98). For these elements, only one stable electronic phase had been obtained in the magnetic case. Ferromagnetic planewave and AE calculations for these gave a  $\Delta$ -Gauge on the order of 1 meV or less, as presented in Fig. 1.

#### 4.5. ONCVP vs PAW

Another methodology for pseudopotential generation is based on the projector augmented wave (PAW) formalism [48]. PAW pseudopotentials have atomic function projectors and pseudoorbitals from which the all-electron (AE) wave function of an electronic state can be recovered, unlike with norm-conserving pseudopotentials. [48] Also, PAW pseudopotentials are included in the class of ultrasoft pseudopotentials, which in turn require lower kinetic energy cut-offs compared to more rigid norm-conserving pseudopotentials. Although PAW faces challenges when being used beyond first-principles calculations, as described in the Introduction section, it is the most accurate pseudization methodology and it is widely used for ground-state calculations.

ONCVP results have been compared with the PAW results obtained using the VASP code. [84–87]. Actually, by the same token, these PAW results are compared with the current AE reference results.

There are only a few actinides for which PAW atomic data are available to perform VASP calculations. Moreover, the details of the electronic configuration of these is known only for Am (Z = 95), Cm (Z = 96), and Cf (Z = 98), as shown in Table 4. As observed from the EOS generated for PAW VASP, the values of  $V_0$  and  $B_0$  are consistent with the results obtained from ONCVP. However, the latter showed much better agreement with AE results, as can be seen in Table 1 and Table 2. Other attempts to produce PAWs for actinides have been proposed in the literature, as suggested by Torres et al. [88,89]. These attempts employ equations of state (EOS) consistent with those used to produce PAWs with VASP.

When it comes to SHEs, in the literature, only the PAW VASP atomic data for the *p*-elements has been made available, by Trombach et al. [90] In this case, fitting the data to produce the EOS PAW VASP showed an unusual behaviour for Cn( $Z = 112$ ) at the suggested kinetic energy cut-off. However, we found a smooth EOS when we increased it to 500 eV. Since we have not succeeded in finding a correct ONCVP capable of generating an EOS that could correctly fit the AE EOS, we have not examined the PAW VASP for the Og element ( $Z = 118$ ) any further. In contrast, for the other SHEs, the  $V_0$  and  $B_0$  obtained by PAW VASP [90] agree reasonably well with the developed ONCVPs, as shown in Table 1 and Table 2, giving confidence in the quality of both the ONCVP and PAW VASP atomic data sets. [90].

## 5. Conclusion

In conclusion, we have generated ONCVPs for thirty-four elements belonging to actinides and super-heavy elements, complementing the eighty-five ONCVPs of the original PseudoDojo project [53]. The new ONCVPs were validated by considering the state-of-the-art descriptors  $\Delta$ -Gauge [54] and  $\Delta_1$ -Gauge [55]. The developed scalar-relativistic ONCVPs for actinides show an average  $\Delta$ -Gauge equal to 0.73 meV indicating a sufficiently high accuracy according to Ref. [102]. For the SHEs we obtained an average  $\Delta$ -Gauge of 1.24 meV showing a good accuracy according to Ref. [102]. The loss of accuracy from actinides to SHEs could be caused by the increase in relativistic effects, which might come from the differences between ZORA without spin-orbit coupling and scalar-relativistic pseudopotential approaches. The developed ONCVPs are characterised by numerous *s*- *p*- *d*- *f*- semicore states, which make these pseudopotentials relatively hard (i.e., high kinetic energy cut-off), but suitable for approaches beyond ground state calculations such as the *GW* approach. The choice of small pseudopotential radii should allow these ONCVPs to be used successfully in high-pressure chemistry as well. Developed ONCVPs provide a pathway for precisely predicting and studying material properties of elements containing actinides and SHEs, even under elevated pressure conditions.

## CRediT authorship contribution statement

Ch. Tantardini and X. Gonze have initiated the project. Ch. Tantardini created the first version and several additional versions of all ONCVP pseudopotentials. The ONCVP pseudopotentials have been refined by M. Giantomassi based on these data to produce the current ones. The ONCVP EOS were produced by M. Giantomassi using the specific PseudoDojo python script that produced the hints and calculated the  $\Delta$ -Gauge and  $\Delta_1$ -Gauge. M. Ilias has produced the AE EOS used as reference, supervised by V. Pershina. A.G. Kvashnin has produced the VASP PAW EOS pseudopotential results. The manuscript has been written through contributions of all authors. All authors have given approval to the final version of the manuscript.

## Declaration of competing interest

The Authors declare no Competing Financial or Non-Financial Interests

## Data availability

The pseudopotential files in their scalar relativistic and full-relativistic version for PBE, PBEsol and LDA are available in the ABINIT psp8 [82,81] and the Quantum ESPRESSO UPF2 formats [103,104] at [github.com/gmatteo/pseudos\\_ac\\_she](https://github.com/gmatteo/pseudos_ac_she). The data coming from AE calculations with the Amsterdam Modelling Suite BAND code are available at the same URL, as well as the input and output files for the generation of ONCVPs. The output from oncvpsp program contains the data for visualisation of  $\ell$ -states with their logarithm derivative with respect to the

energy for both the pseudowavefunctions and AE wavefunctions. It contains also the energy cut-off for each pseudo- $\ell$ -state. These data can be visualised with the gnu-plot script in [github.com/oncvpsp/oncvpsp](https://github.com/oncvpsp/oncvpsp). Furthermore, we have included all data to generate the PBE equation of states for both scalar relativistic ONCVP and ZORA AE and the subsequent files to compute the  $\Delta$ -Gauge and the  $\Delta_1$ -Gauge.

## Acknowledgements

Ch.T. acknowledges support from the Research Council of Norway (262695, 324590). M. I. thanks the HIM for the financial support through the Visiting Scholar Agreement and for the support of the Slovak Research and Development Agency (APVV-20-0098). M. I. was partially supported by the grant of Ministry of Science and Higher Education of the Russian Federation, Nr. 075-10-2020-117. The authors would like to acknowledge Pier Philipsen of Amsterdam Model Suite BAND for his support with the all-electron calculations and Davide Ceresoli of CNR of Milano for the generation of UPF2 format of ONCVP for Quantum ESPRESSO.

## References

- [1] L. Boeri, R. Hennig, P. Hirschfeld, G. Profeta, A. Sanna, E. Zurek, W.E. Pickett, M. Amsler, R. Dias, M.I. Eremets, C. Heil, R.J. Hemley, H. Liu, Y. Ma, C. Pierleoni, A.N. Kolmogorov, N. Rybin, D. Novoselov, V. Anisimov, A.R. Oganov, C.J. Pickard, T. Bi, R. Arita, I. Errea, C. Pellegrini, R. Requist, E.K.U. Gross, E.R. Margine, S.R. Xie, Y. Quan, A. Hire, L. Fanfarillo, G.R. Stewart, J.J. Hamlin, V. Stanev, R.S. Gonnelli, E. Piatti, D. Romanin, D. Daghero, R. Valenti, The 2021 room-temperature superconductivity roadmap, *J. Phys. Condens. Matter* 34 (18) (2022) 183002.
- [2] V. Struzhkin, B. Li, C. Ji, X.-J. Chen, V. Prakapenka, E. Greenberg, I. Troyan, A. Gavriliuk, H.-k. Mao, Superconductivity in La and Y hydrides: remaining questions to experiment and theory, *Matter Radiat. Extrem.* 5 (2) (2020) 028201.
- [3] D.V. Semenok, I.A. Kruglov, A.G. Kvashnin, A.R. Oganov, On distribution of superconductivity in metal hydrides, *Curr. Opin. Solid State Mater. Sci.* 7 (2020) 100808.
- [4] I. Trojan, D. Semenok, A. Ivanova, A. Kvashnin, D. Zhou, A. Sadakov, O. Sobolevsky, V. Pudalov, I. Lyubutin, A. Oganov, High-temperature superconductivity in hydrides, *Phys. Usp.* 65 (7) (2022) 748–761, <https://ufn.ru/en/articles/2022/7/h/>.
- [5] M. Kumar, M. Pokhriyal, M. Gupta, G. Vijaya Prakash, S. Uma, R. Nagarajan, Optical property evaluation of thoria doped with heavier rare-earth oxides  $\text{Ln}_{0.5}$  ( $\text{Ln} = \text{Er}^{3+}$ ,  $\text{Ho}^{3+}$ ,  $\text{Tm}^{3+}$ , and  $\text{Yb}^{3+}$ ), *J. Am. Ceram. Soc.* 102 (4) (2019) 1832–1842.
- [6] I. Usov, M. Šýkora, Uranium oxide solar cells, <https://patents.google.com/patent/US20170018673A1/en>, 2017.
- [7] A.M. Adamska, E.L. Bright, J. Sutcliffe, W. Liu, O.D. Payton, L. Picco, T.B. Scott, Characterisation of electrodeposited polycrystalline uranium dioxide thin films on nickel foil for industrial applications, *Thin Solid Films* 597 (2015) 57–64, <https://doi.org/10.1016/j.tsf.2015.11.030>.
- [8] R.K. Willardson, J.W. Moody, H.L. Goering, The electrical properties of uranium oxides, *J. Inorg. Nucl. Chem.* 6 (1) (1958) 19–33.
- [9] C.A. Kruschwitz, S. Mukhopadhyay, D. Schwellenbach, T. Meek, B. Shaver, T. Cunningham, J.P. Auxier, Semiconductor Neutron Detectors Using Depleted Uranium Oxide, Hard X-Ray, Gamma-Ray, and Neutron Detector Physics XVI, vol. 9213, SPIE, 2014, pp. 44–52.
- [10] M. Khilla, S. El-Fekey, M. El-Mamoon Yahia, Electrical conductivity of some uranium oxides in the composition range  $\text{UO}_3 - \text{U}_3\text{O}_{8-z}$ , *Radiochim. Acta* 28 (2) (1981) 115–117.
- [11] L. Ding, J. Leduc, T. Fischer, S. Mathur, Y. Li, Gelation of uranyl ions and gel-derived uranium oxide nanoparticles for gas sensing, *Nanoscale Adv.* 2 (6) (2020) 2478–2484.
- [12] A. Peña-Duarte, A.J. Acevedo-González, R.M. Lagle, M. Drabo, S.U. Egariwwe, C.R. Cabrera, Stable Uranium Oxide Under Atmospheric Conditions: An Electroplating Technique for U Film Fabrication at Boron-Doped Diamond Electrodes, *ACS Materials, Au*, 2023.
- [13] P. Li, Z. Lu, J. Wang, T. He, N. Ou, J. Liang, Q. Fan, XPS determination of the uranium valences in  $\text{U}_3\text{O}_8$ , *Nucl. Anal.* (2023) 100071.
- [14] H. Dong, R. Wang, D. Zhang, T. Shi, Y. Lou, X. Fu, Y. Zhong, L. Lu, B. Su, L. Zhu, et al., Effect of annealing temperature on electronic band structural, optical constant, and band gap of uranium dioxide films, *Mater. Sci. Eng. B* 293 (2023) 116496.
- [15] C. Colmenares, K. Terada, The adsorption of carbon dioxide on uranium and plutonium oxides, *J. Nucl. Mater.* 58 (3) (1975) 336–356.
- [16] D. Larson, AES and XPS study of plutonium oxidation, *J. Vac. Sci. Technol.* 17 (1) (1980) 55–58.
- [17] J. Tang, J. Chen, P. Liu, R. Qiu, First principles study of oxygen diffusion in plutonium dioxide, sesquioxide, and their interface under activated conditions, *J. Nucl. Mater.* 578 (2023) 154348.

- [18] J. Shi, T. Gao, G. Li, H. Wang, W. Luo, Insight into the effect of coexistence of  $\text{CO}_2$  and  $\text{H}_2$  on stoichiometric and defective  $\text{PuO}_2$  surfaces hydriding from first-principles study, *J. Vac. Sci. Technol. A* 41 (4) (2023).
- [19] L.N. Dinh, S.B. Donald, J.A. Stanford, C.K. Saw, R. Gollott, J.M. Haschke, W. McLean, The kinetics of the  $\text{PuO}_2$  to  $\text{Pu}_2\text{O}_3$  conversion, *J. Chem. Phys.* 158 (13) (2023).
- [20] C.E. Düllmann, E. Artes, A. Dragoun, R. Haas, E. Jäger, B. Kindler, B. Lommel, K.-M. Mangold, C.-C. Meyer, C. Mokry, et al., Advancements in the fabrication and characterization of actinide targets for superheavy element production, *J. Radioanal. Nucl. Chem.* 332 (5) (2023) 1505–1514.
- [21] A. Das, U. Das, A.K. Das, Relativistic effects on the chemical bonding properties of the heavier elements and their compounds, *Coord. Chem. Rev.* 479 (2023) 215000.
- [22] L. Zhu, Law of optimal incident energy for synthesizing superheavy elements in hot fusion reactions, *Phys. Rev. Res.* 5 (2) (2023) L022030.
- [23] E. Holmbeck, T. Sprouse, M. Mumpower, Nucleosynthesis and observation of the heaviest elements, *Eur. Phys. J. A* 59 (2) (2023) 28.
- [24] A. Türler, R. Eichler, A. Yakushev, Chemical studies of elements with  $Z \geq 104$  in gas phase, *Nucl. Phys. A* 944 (2015) 640–689.
- [25] V. Pershina, A relativistic periodic DFT study on interaction of superheavy elements 112 (Cn) and 114 (Fl) and their homologs Hg and Pb, respectively, with a quartz surface, *Phys. Chem. Chem. Phys.* 18 (26) (2016) 17750–17756.
- [26] S. Dmitriev, Superheavy element factory, in: *Fission and Properties of Neutron-Rich Nuclei-Proceedings of the Sixth International Conference on Icf6*, World Scientific, 2017, p. 109.
- [27] A. Zaitsevskii, C. van Wüllen, A.V. Titov, Communications: adsorption of element 112 on the gold surface: many-body wave function versus density functional theory, *J. Chem. Phys.* 132 (8) (2010).
- [28] W. Nazarewicz, The limits of nuclear mass and charge, *Nat. Phys.* 14 (6) (2018) 537–541.
- [29] M. Aydinol, Electron impact excitation of single 105Db, 106Sg, 107Bh, 108Hs, 109Mt, 110Ds, 111Rg, 112Cn, 113Uut, 114Fl, 115Uup, 116Lv, 117Uus, 118Uuo atoms O subshell ionization cross sections by using Lotz's equation, *AIP Conf. Proc.* 2178 (1) (2019) 030024.
- [30] A. Såmark-Roth, D. Cox, D. Rudolph, L. Sarmiento, M. Albertsson, B. Carlsson, J. Egido, P. Golubev, J. Heery, A. Yakushev, et al., Spectroscopy along flerovium decay chains. III. Details on experiment, analysis,  $^{282}\text{Cn}$ , and spontaneous fission branches, *Phys. Rev. C* 107 (2) (2023) 024301.
- [31] Z. Matheson, S.A. Giuliani, W. Nazarewicz, J. Sadhukhan, N. Schunck, Cluster radioactivity of  $^{294}_{118}\text{og}_{176}$ , arXiv preprint arXiv:1812.06490, 2018.
- [32] L.G.M. de Macedo, C.A.B. Negrão, R.M. de Oliveira, R.F. de Menezes, F. Pirani, R. Gargano, The van der Waals interactions in systems involving superheavy elements: the case of oganesson ( $Z = 118$ ), *Phys. Chem. Chem. Phys.* 25 (1) (2023) 633–645.
- [33] M.R. Pederson, A.I. Johnson, K.P. Withanage, S. Dolma, G.B. Flores, Z. Hooshmand, K. Khandal, P.O. Lasode, T. Baruah, K.A. Jackson, Downward quantum learning from element 118: automated generation of Fermi-Löwdin orbitals for all atoms, *J. Chem. Phys.* 158 (8) (2023).
- [34] A. Ryzhkov, V. Pershina, M. Ilić, V. Shabaev, A theoretical study of the adsorption behaviour of superheavy 7p-elements and their compounds on a surface of gold in comparison with their lighter homologs, *Phys. Chem. Chem. Phys.* 25 (22) (2023) 15362–15370.
- [35] P. Jerabek, B. Schuetzrumpf, P. Schwerdtfeger, W. Nazarewicz, Electron and nucleon localization functions of oganesson: approaching the Thomas-Fermi limit, *Phys. Rev. Lett.* 120 (5) (2018) 053001.
- [36] C.S. Nash, Atomic and molecular properties of elements 112, 114, and 118, *J. Phys. Chem. A* 109 (15) (2005) 3493–3500.
- [37] X. Dong, A.R. Oganov, A.F. Goncharov, E. Stavrou, S. Lobanov, G. Saleh, G.-R. Qian, Q. Zhu, C. Gatti, V.L. Deringer, et al., A stable compound of helium and sodium at high pressure, *Nat. Chem.* 9 (5) (2017) 440–445.
- [38] H.P.A. Mercier, M.R. Bortolus, G.J. Schrobilgen, 1.08 - noble-gas chemistry, in: J. Reedijk, K.R. Poepelmeier (Eds.), *Comprehensive Inorganic Chemistry III*, third edition, Elsevier, Oxford, 2023, pp. 439–526, <https://www.sciencedirect.com/science/article/pii/B9780128231449001667>.
- [39] Z. Liu, Y. Bai, O. Fernando, C. Pickard, D. Yan, H.-Q. Lin, M. Miao, Helium reaction with sodium halides under pressure, in: *APS March Meeting Abstracts*, vol. 2019, 2019, pp. L17–007.
- [40] J. Shi, W. Cui, J. Hao, M. Xu, X. Wang, Y. Li, Formation of ammonia–helium compounds at high pressure, *Nat. Commun.* 11 (1) (2020) 3164.
- [41] B. Monserrat, M. Martinez-Canales, R.J. Needs, C.J. Pickard, Helium-iron compounds at terapascal pressures, *Phys. Rev. Lett.* 121 (1) (2018) 015301.
- [42] J. Zhang, J. Lv, H. Li, X. Feng, C. Lu, S.A. Redfern, H. Liu, C. Chen, Y. Ma, Rare helium-bearing compound  $\text{FeO}_2$  stabilized at deep-earth conditions, *Phys. Rev. Lett.* 121 (25) (2018) 255703.
- [43] H. Gao, C. Liu, A. Hermann, R.J. Needs, C.J. Pickard, H.-T. Wang, D. Xing, J. Sun, Coexistence of plastic and partially diffusive phases in a helium-methane compound, *Nat. Sci. Rev.* 7 (10) (2020) 1540–1547.
- [44] M.-S. Miao, X.-L. Wang, J. Brgoč, F. Spera, M.G. Jackson, G. Kresse, H.-Q. Lin, Anionic chemistry of noble gases: formation of Mg-NG (NG = Xe, Kr, Ar) compounds under pressure, *J. Am. Chem. Soc.* 137 (44) (2015) 14122–14128.
- [45] H. Gao, J. Sun, C.J. Pickard, R.J. Needs, Prediction of pressure-induced stabilization of noble-gas-atom compounds with alkali oxides and alkali sulfides, *Phys. Rev. Mater.* 3 (1) (2019) 015002.
- [46] X.-S. Liu, Chapter 6 - inorganic photochemical synthesis, in: R. Xu, Y. Xu (Eds.), *Modern Inorganic Synthetic Chemistry*, second edition, Elsevier, Amsterdam, 2017, pp. 143–165, <https://www.sciencedirect.com/science/article/pii/B9780444635914000069>.
- [47] F. Bloch, Über die Quantenmechanik der Elektronen in Kristallgittern, *Z. Phys.* 52 (7) (1929) 555–600, <https://doi.org/10.1007/BF01339455>.
- [48] P.E. Blöchl, Projector augmented-wave method, *Phys. Rev. B* 50 (1994) 17953–17979.
- [49] J. Zwanziger, Computation of NMR observables: consequences of projector-augmented wave sphere overlap, *Solid State Nucl. Magn. Reson.* 80 (2016) 14–18.
- [50] L. Hedin, New method for calculating the one-particle Green's function with application to the electron-gas problem, *Phys. Rev. A* 139 (1965) 795.
- [51] E.E. Salpeter, H.A. Bethe, A relativistic equation for bound-state problems, *Phys. Rev.* 84 (1951) 1232–1242.
- [52] G. Brunin, H.P.C. Miranda, M. Giantomassi, M. Royo, M. Stengel, M.J. Verstraete, X. Gonze, G.-M. Rignanese, G. Hautier, Phonon-limited electron mobility in Si, GaAs, and GaP with exact treatment of dynamical quadrupoles, *Phys. Rev. B* 102 (2020) 094308.
- [53] M. van Setten, M. Giantomassi, E. Bousquet, M. Verstraete, D. Hamann, X. Gonze, G.-M. Rignanese, The pseudodojo: training and grading a 85 element optimized norm-conserving pseudopotential table, *Comput. Phys. Commun.* 226 (2018) 39–54.
- [54] K. Lejaeghere, V.V. Speybroeck, G.V. Oost, S. Cottenier, Error estimates for solid-state density-functional theory predictions: an overview by means of the ground-state elemental crystals, *Crit. Rev. Solid State Mater. Sci.* 39 (1) (2014) 1–24.
- [55] F. Jollet, M. Torrent, N. Holzwarth, Generation of projector augmented-wave atomic data: a 71 element validated table in the XML format, *Comput. Phys. Commun.* 185 (4) (2014) 1246–1254.
- [56] D.R. Hamann, Optimized norm-conserving Vanderbilt pseudopotentials, *Phys. Rev. B* 88 (2013) 085117.
- [57] D.R. Hamann, Erratum: optimized norm-conserving Vanderbilt pseudopotentials, *Phys. Rev. B* 88 (2013) 085117, *Phys. Rev. B* 95 (2017) 239906.
- [58] S.G. Louie, S. Froyen, M.L. Cohen, Nonlinear ionic pseudopotentials in spin-density-functional calculations, *Phys. Rev. B* 26 (4) (1982) 1738.
- [59] M. Teter, Additional condition for transferability in pseudopotentials, *Phys. Rev. B* 48 (8) (1993) 5031.
- [60] R. Hansel, C. Brock, B. Paikoff, A. Tackett, D. Walker, Automated generation of highly accurate, efficient and transferable pseudopotentials, *Comput. Phys. Commun.* 196 (2015) 267.
- [61] D.D. Koelling, B.N. Harmon, A technique for relativistic spin-polarised calculations, *J. Phys. C, Solid State Phys.* 10 (16) (1977) 3107.
- [62] T. Takeda, The scalar relativistic approximation, *Z. Phys. B, Condens. Matter* 32 (1) (1978) 43–48.
- [63] F. Birch, Finite elastic strain of cubic crystals, *Phys. Rev.* 71 (11) (1947) 809.
- [64] M. Filatov, D. Cremer, On the physical meaning of the ZORA hamiltonian, *Mol. Phys.* 101 (14) (2003) 2295–2302.
- [65] C. Chang, M. Pelizzier, P. Durand, Regular two-component Pauli-like effective Hamiltonians in Dirac theory, *Phys. Scr.* 34 (5) (1986) 394.
- [66] J.-L. Heully, I. Lindgren, E. Lindroth, S. Lundqvist, A.-M. Martensson-Pendrill, Diagonalisation of the Dirac hamiltonian as a basis for a relativistic many-body procedure, *J. Phys. B, At. Mol. Phys.* 19 (18) (1986) 2799.
- [67] E.v. Lenthe, E.-J. Baerends, J.G. Snijders, Relativistic regular two-component hamiltonians, *J. Chem. Phys.* 99 (6) (1993) 4597–4610.
- [68] E. van Lenthe, E.-J. Baerends, J.G. Snijders, Relativistic total energy using regular approximations, *J. Chem. Phys.* 101 (11) (1994) 9783–9792.
- [69] W.P. Huhn, V. Blum, One-hundred-three compound band-structure benchmark of post-self-consistent spin-orbit coupling treatments in density functional theory, *Phys. Rev. Mater.* 1 (2017) 033803.
- [70] J.P. Perdew, M. Ernzerhof, K. Burke, Rationale for mixing exact exchange with density functional approximations, *J. Chem. Phys.* 105 (1996) 9982.
- [71] G. te Velde, E.J. Baerends, Precise density-functional method for periodic structures, *Phys. Rev. B* 44 (1991) 7888–7903.
- [72] P. Philipsen, G. te Velde, E. Baerends, J. Berger, P. de Boeij, M. Franchini, J. Groenveld, E. Kadantsev, R. Klooster, F. Kootstra, M. Pols, P. Romaniello, M. Raupach, D. Skachkov, J. Smidjev, C. Verzijl, C. G. J. A. J.M. Thijssen, G. Wiesenecker, C.A. Peebles, G. Schreckenbach, T. Ziegler, sCM, *Theoretical Chemistry*, Vrije Universiteit, Amsterdam, the Netherlands, <http://www.scm.com>, 2023.
- [73] G. Wiesenecker, G. te Velde, E.J. Baerends, Analytic quadratic integration over the two-dimensional Brillouin zone, *J. Phys. C, Solid State Phys.* 21 (23) (1988) 4263.
- [74] G. Wiesenecker, E.J. Baerends, Quadratic integration over the three-dimensional Brillouin zone, *J. Phys. Condens. Matter* 3 (35) (1991) 6721.
- [75] M. Franchini, P.H.T. Philipsen, L. Visscher, The Becke fuzzy cells integration scheme in the Amsterdam density functional program suite, *J. Comput. Chem.* 34 (21) (2013) 1819–1827.
- [76] M. Franchini, P.H.T. Philipsen, L. Visscher, Accurate Coulomb potentials for periodic and molecular systems through density fitting, *J. Chem. Theory Comput.* 10 (5) (2014) 1994–2004.

- [77] C.G. Broyden, The convergence of a class of double-rank minimization algorithms 1. General considerations, *IMA J. Appl. Math.* 6 (1970) 76–90.
- [78] D.F. Shanno, Conditioning of quasi-Newton methods for function minimization, *Math. Comput.* 24 (111) (1970) 647–656.
- [79] D. Goldfarb, A family of variable-metric methods derived by variational means, *Math. Comput.* 24 (109) (1970) 23–26.
- [80] T. Steihaug, Practical Methods of Optimization. Volume 1: Unconstrained Optimization, vol. 12 (4), Wiley, New York, 1980, by R. Fletcher.
- [81] X. Gonze, F. Jollet, F.A. Araujo, D. Adams, B. Amadon, T. Applencourt, C. Audouze, J.-M. Beuken, J. Bieder, A. Bokhanchuk, E. Bousquet, F. Bruneval, D. Caliste, M. Côté, F. Dahm, F.D. Pieve, M. Delaveau, M.D. Gennaro, B. Dorado, C. Espejo, G. Geneste, L. Genovese, A. Gerossier, M. Giantomassi, Y. Gillet, D. Hamann, L. He, G. Jomard, J.L. Janssen, S.L. Roux, A. Levitt, A. Lherbier, F. Liu, I. Lukáčević, A. Martin, C. Martins, M. Oliveira, S. Poncé, Y. Pouillon, T. Rangel, G.-M. Rignanese, A. Romero, B. Rousseau, O. Rubel, A. Shukri, M. Stankovski, M. Torrent, M.V. Setten, B.V. Troeye, M. Verstraete, D. Waroquiers, J. Wiktor, B. Xue, A. Zhou, J. Zwanziger, Recent developments in the ABINIT software package, *Comput. Phys. Commun.* 205 (2016) 106–131.
- [82] X. Gonze, B. Amadon, G. Antonius, F. Arnardi, L. Baguet, J.-M. Beuken, J. Bieder, F. Bottin, J. Bouchet, E. Bousquet, N. Brouwer, F. Bruneval, G. Brunin, T. Cavignac, J.-B. Charraud, W. Chen, M. Côté, S. Cottenier, J. Denier, G. Geneste, P. Ghosez, M. Giantomassi, Y. Gillet, O. Gingras, D.R. Hamann, G. Hautier, X. He, N. Helbig, N. Holzwarth, Y. Jia, F. Jollet, W. Lafargue-Dit-Hauret, K. Lejaeghere, M.A.L. Marques, A. Martin, C. Martins, H.P.C. Miranda, F. Naccarato, K. Persson, G. Petretto, V. Planes, Y. Pouillon, S. Prokhortenko, F. Ricci, G.-M. Rignanese, A.H. Romero, M.M. Schmitt, M. Torrent, M.J. van Setten, B. Van Troeye, M.J. Verstraete, G. Zérâah, J.W. Zwanziger, The Abinit project: impact, environment and recent developments, *Comput. Phys. Commun.* 248 (2020) 107042.
- [83] A.H. Romero, D.C. Allan, B. Amadon, G. Antonius, T. Applencourt, L. Baguet, J. Bieder, F. Bottin, J. Bouchet, E. Bousquet, F. Bruneval, G. Brunin, D. Caliste, M. Côté, J. Denier, C. Dreyer, P. Ghosez, M. Giantomassi, Y. Gillet, O. Gingras, D.R. Hamann, G. Hautier, F. Jollet, G. Jomard, A. Martin, H.P.C. Miranda, F. Naccarato, G. Petretto, N.A. Pike, V. Planes, S. Prokhortenko, T. Rangel, F. Ricci, G.-M. Rignanese, M. Royo, M. Stengel, M. Torrent, M.J. van Setten, B. Van Troeye, M.J. Verstraete, J. Wiktor, J.W. Zwanziger, X. Gonze, Abinit: overview and focus on selected capabilities, *J. Chem. Phys.* 152 (12) (2020) 124102.
- [84] G. Kresse, J. Furthmüller, Efficient iterative schemes for ab initio total-energy calculations using a plane-wave basis set, *Phys. Rev. B* 54 (16) (1996) 11169.
- [85] G. Kresse, J. Hafner, Ab initio molecular dynamics for liquid metals, *Phys. Rev. B* 47 (1) (1993) 558–561.
- [86] G. Kresse, J. Furthmüller, Ab initio molecular-dynamics simulation of the liquid-metal-amorphous-semiconductor transition in germanium, *Phys. Rev. B* 49 (20) (1994) 14251.
- [87] J. Hafner, Ab-initio simulations of materials using VASP: density-functional theory and beyond, *J. Comput. Chem.* 29 (13) (2008) 2044–2078, <https://doi.org/10.1002/jcc.21057>.
- [88] E. Torres, T. Kaloni, Projector augmented-wave pseudopotentials for uranium-based compounds, *Comput. Mater. Sci.* 171 (2020) 109237.
- [89] E. Torres, T. Kaloni, Projector augmented-wave pseudopotentials for the actinide elements (Ac–Bk), *J. Nucl. Mater.* 553 (2021) 153031.
- [90] L. Trombach, S. Ehlert, S. Grimme, P. Schwerdtfeger, J.-M. Mewes, Exploring the chemical nature of super-heavy main-group elements by means of efficient plane-wave density-functional theory, *Phys. Chem. Chem. Phys.* 21 (2019) 18048–18058.
- [91] X. Gonze, P. Käckell, M. Scheffler, Ghost states for separable, norm-conserving, ab initio pseudopotentials, *Phys. Rev. B* 41 (17) (1990) 12264–12267.
- [92] X. Gonze, R. Stumpf, M. Scheffler, Analysis of separable potentials, *Phys. Rev. B* 44 (16) (1991) 8503–8513.
- [93] H. Manjunatha, Y. Vidyā, P.D. Gupta, N. Manjunatha, N. Sowmya, L. Seenappa, T. Nandi, Rules of thumb for synthesizing superheavy elements, *J. Phys. G, Nucl. Part. Phys.* 49 (12) (2022) 125101.
- [94] H. Manjunatha, Y. Vidyā, P. Gupta, N. Manjunatha, N. Sowmya, L. Seenappa, T. Nandi, Exploring an experimental route of synthesizing superheavy elements beyond Z > 118, arXiv preprint, arXiv:2108.08335, 2021.
- [95] X.-L. He, X. Dong, Q. Wu, Z. Zhao, Q. Zhu, A.R. Oganov, Y. Tian, D. Yu, X.-F. Zhou, H.-T. Wang, Predicting the ground-state structure of sodium boride, *Phys. Rev. B* 97 (10) (2018) 100102.
- [96] G. Saleh, A. Oganov, Alkali subhalides: high-pressure stability and interplay between metallic and ionic bonds, *Phys. Chem. Chem. Phys.* 18 (4) (2016) 2840–2849.
- [97] M.R. Kibler, From the Mendeleev periodic table to particle physics and back to the periodic table, *Found. Chem.* 9 (2007) 221–234.
- [98] F. Guérard, C. Maingueneau, L. Liu, R. Eychenne, J.-F. Gestin, G. Montavon, N. Galland, Advances in the chemistry of astatine and implications for the development of radiopharmaceuticals, *Acc. Chem. Res.* 54 (16) (2021) 3264–3275.
- [99] D.S. Wilbur, Enigmatic astatine, *Nat. Chem.* 5 (3) (2013) 246.
- [100] J. Champion, M. Seydou, A. Sabatié-Gogova, E. Renault, G. Montavon, N. Galland, Assessment of an effective quasirelativistic methodology designed to study astatine chemistry in aqueous solution, *Phys. Chem. Chem. Phys.* 13 (33) (2011) 14984–14992.
- [101] G.W. Visser, E.L. Diemer, Inorganic astatine chemistry: formation of complexes of astatine, *Radiochim. Acta* 33 (2–3) (1983) 145–152.
- [102] K. Lejaeghere, G. Bihlmayer, T. Bjorkman, P. Blaha, S. Blugel, V. Blum, D. Caliste, I.E. Castelli, S.J. Clark, A. Dal Corso, S. de Gironcoli, T. Deutsch, J.K. Dewhurst, I. Di Marco, C. Draxl, M. Dulak, O. Eriksson, J.A. Flores-Livas, K.F. Garrity, L. Genovese, P. Giannozzi, M. Giantomassi, S. Goedecker, X. Gonze, O. Granas, E.K.U. Gross, A. Gulans, F. Gygi, D.R. Hamann, P.J. Hasnip, N.A.W. Holzwarth, D. Iuskan, D.B. Jochym, F. Jollet, D. Jones, G. Kresse, K. Koepernik, E. Küçükbenli, Y.O. Kvashnin, I.I.M. Locht, S. Lubeck, M. Marsman, N. Marzari, U. Nitzsche, L. Nordstrom, T. Ozaki, L. Paulatto, C.J. Pickard, W. Poelmans, M.I.J. Probert, K. Refson, M. Richter, G.-M. Rignanese, S. Saha, M. Scheffler, M. Schlipf, K. Schwarz, S. Sharma, F. Tavaizza, P. Thunstrom, A. Tkatchenko, M. Torrent, D. Vanderbilt, M. van Setten, V. Van Speybroeck, J.M. Wills, J.R. Yates, G.-X. Zhang, S. Cottenier, Reproducibility in density functional theory calculations of solids, *Science* 351 (6280) (2016) aad3000.
- [103] P. Giannozzi, S. Baroni, N. Bonini, M. Calandra, R. Car, C. Cavazzoni, D. Ceresoli, G.L. Chiarotti, M. Cococcioni, I. Dabo, A.D. Corso, S. de Gironcoli, S. Fabris, G. Fratesi, R. Gebauer, U. Gerstmann, C. Gougoussis, A. Kokalj, M. Lazzeri, L. Martin-Samos, N. Marzari, F. Mauri, R. Mazzarello, S. Paolini, A. Pasquarello, L. Paulatto, C. Sbraccia, S. Scandolo, G. Scalauzero, A.P. Seitsonen, A. Smogunov, P. Umari, R.M. Wentzcovitch, QUANTUM ESPRESSO: a modular and open-source software project for quantum simulations of materials, *J. Phys. Condens. Matter* 21 (39) (2009) 395502.
- [104] P. Giannozzi, O. Andreussi, T. Brummel, O. Bunau, M.B. Nardelli, M. Calandra, R. Car, C. Cavazzoni, D. Ceresoli, M. Cococcioni, N. Colonna, I. Carnimeo, A.D. Corso, S.d. Gironcoli, P. Delugas, R.A. DiStasio, A. Ferretti, A. Floris, G. Fratesi, G. Fugallo, R. Gebauer, U. Gerstmann, F. Giustino, T. Gorni, J. Jia, M. Kawamura, H.-Y. Ko, A. Kokalj, E. Küçükbenli, M. Lazzeri, M. Marsili, N. Marzari, F. Mauri, N.L. Nguyen, H.-V. Nguyen, A. Otero-de-la Roza, L. Paulatto, S. Poncé, D. Rocca, R. Sabatini, B. Santra, M. Schlipf, A.P. Seitsonen, A. Smogunov, I. Timrov, T. Thonhauser, P. Umari, N. Vast, X. Wu, S. Baroni, Advanced capabilities for materials modelling with Quantum ESPRESSO, *J. Phys. Condens. Matter* 29 (46) (2017) 465901.